Journal of Hydrology 632 (2024) 130953

Contents lists available at ScienceDirect

Journal of Hydrology

journal homepage: www.elsevier.com/locate/jhydrol

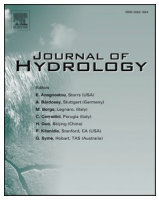

Influence of karst conduit's geometry and morphology on 3D flow and transport processes: Insights from 3D tracer tests and numerical modelling

Mohammed Aliouache [a,*], Pierre Fischer [b], Pascal Brunet [a], Lionel Lapierre [c], Benoit Ropars [d], Frank Vasseur [e], Hervé Jourde [a,*]

[a] HydroSciences Montpellier (HSM), University of Montpellier, CNRS, IRD, Montpellier, France
[b] IC2MP, Université de Poitiers, CNRS UMR 7285, HydrASA, Poitiers, France
[c] LIRMM, University of Montpellier, CNRS-UM UMR 5506, Montpellier, France
[d] REEDS, Solutions robotisées d'inspection subaquatique, Montpellier, France
[e] Association CELADON, Exploration spéléologique en plongée, Hérault, France

ARTICLE INFO

This manuscript was handled by Corrado Corradini, Editor-in-Chief, with the assistance of Junbing Pu, Associate Editor

Keywords:
Karst
Tracer test
Conduit geometry
Conduit morphology
Solute transport

ABSTRACT

In karst, the characterization of subsurface solute and contaminant transport is a major issue that has been widely investigated due to the high vulnerability of these hydrosystems. In former studies, several researchers addressed these needs with different approaches such as laboratory experiments, field experiments, or groundwater flow and transport simulations. The objective of such approaches is to improve knowledge of transport processes in karst hydrosystems, and propose solutions to limit the downstream hydrogeological risks (contamination of water resources). In this study, we performed the 3D mapping of the karst conduit, which outlet is the Lez spring (southern France) to get the precise geometry and morphology of this fully water-filled karst conduit. Then we injected a dye in the water-filled karst conduit and performed a continuous monitoring of dye tracer recovery at three different cross-sections located downstream the injection spot, at a distance of 40 m, 90 m and 160 m, respectively. In each cross-section, five submersible fluorometer probes were positioned at different locations (top, right, down, left and central parts) along the cross-section of the karst conduit. Experimental data allowed to reconstruct the transient spatial distribution of concentration for each cross-section, which allowed assessing the propagation and evolution of solute plume over time. Monitored data also provided information about dye mixing along the karst conduit and were used to investigate the effect of karst conduit geometry, flow turbulences and velocity profiles on the mixing processes and propagation of solute plume along the conduit with numerical models. Modelling results showed that the consideration of 3D mapped karst conduit geometry and morphology allows a much better reproduction of observed transport processes and breakthrough curves, than the one obtain when considering simplified conduit geometry and morphology.

1. Introduction

Karst aquifers provide about 22 % of freshwater resources in the European continent. Several big cities are supplied by freshwater from karst aquifers (Hartmann et al., 2014). However, such systems are very complex and its hydrodynamics are very challenging to predict. Also, karst aquifers are highly vulnerable to contamination, due to the existence of rapid flows, and fast transport via conduits to karst springs (Ford and Williams, 2007; Goldscheider and Drew, 2014). Karst aquifers are mainly characterized by open conduits which provide low resistance pathways for groundwater flow. Such highly conductive pathways often make flow through the matrix negligible in these systems. Karst springs represent the natural outlets of conduit networks in karstified aquifers. A spring is a place where water moving underground finds an opening to the land surface after a rain, and sometimes in a continuous flow (White, 1988). In most karst aquifers, flows in secondary conduits converge into a main conduit that discharges through a single large spring (White, 1999). In karst groundwater systems, the existence of several features, such as conduits, fissures, fractures and matrix results on a complicated internal structure of the aquifer (Morales et al., 2010; Zhao et al., 2011; Sharma et al., 2013). Thus, exposing geometric features and characterizing the hydrodynamics of karst aquifers through one or more methods

* Corresponding authors.
E-mail addresses: mohammed.aliouache@umontpellier.fr (M. Aliouache), herve.jourde@umontpellier.fr (H. Jourde).

https://doi.org/10.1016/j.jhydrol.2024.130953
Received 13 October 2023; Received in revised form 26 December 2023; Accepted 9 February 2024
Available online 28 February 2024

are an important purpose of karst hydrogeology works.

Flow tracing with fluorescent dyes became very relevant to investigate water fluxes in karst flow systems. Most of the time, hydrologists inject fluorescent dye at the surface, often at rivers or sinkhole inlets, and monitor the evolution of dye concentration at springs. Such experiments provide a global information about flow direction and velocity. However, the karst system often remains a black box and solute transport mechanism at local scale is ignored. This tracer test informs on hydraulic characteristics of conduits between two specific points of recharge and discharge. Flury and Wai (2003) described an ideal water tracer as one that (1) is relatively conservative and doesn't show losses through sorption; (2) is stable and doesn't interact with the water; (3) can be easily detected even at low concentrations; and (4) shows no threat to the environment and has no toxicity. Several dyes have been used as hydrological tracers and the common ones are probably Fluorescein/Uranine and Rhodamine WT. The detection limit of uranine, for example, is as low as 2 $\mu g/m^3$ (Käss, 1998). Dyes can often be visually detected in water at parts-per-million concentrations, whereas more advanced tools are required to detect much lower concentrations, sometimes continuously, which allows to obtain breakthrough curves (BTC) at karst spring or more specific location. Recently, manufacturers such as Traqua, Turner Designs and Yellow Springs Instruments have introduced submersible fluorometers that can be used for in-situ continuous-flow monitoring. Continuous-flow fluorometry provides significant advantages for quantitative dye-tracer tests; it allows to obtain dye BTC with minimum bias (Smart, 1988). Obtaining a BTC with a high restitution rate during the test significantly increases the confidence that the injected tracer passed through and results are of a good quality and ready for interpretation. Analysis of the BTC (measured dye concentration over time) represents an effective way to assess conduit-flow and solute transport characteristics in karst aquifers. Kincaid et al. (2005) listed some relevant information that could be extracted from a BTC curve of a tracer test (e.g. mean flow velocity using the peak concentration time; tracer restitution by integrating the surface under the curve; hydro-dispersive properties by evaluating the shape of the curve). The most important characteristics of the BTC include the first arrival time, time to peak concentration, elapsed time of passage of the dye plume, and the shape of the BTC tail (recession phase). Breakthrough curves obtained from a tracer test may provide relevant information about the hydraulic properties of the conduit as well as the effect of its geometry and its morphology on transport processes. In general, tracer tests results showing long-tailed BTCs cannot be described by the classical advection–dispersion equation (ADE) (Barberá et al., 2018; Goldscheider, 2008). The long tailed BTC is often explained by the influence of subsurface ponds or other immobile regions along the flow path, and/or exchange with the surrounding fractured rock matrix.

In order to better assess karst systems hydrodynamics, different models were applied to simulate flow and transport processes. For instance, lumped parameter models are widely used to simulate the discharge dynamics of karst springs. These models are relatively simple, low cost and require easy to acquire data (Fleury et al., 2007a,b; Hartmann et al., 2014). However, such models cannot capture the complex flow and transport processes. In contrast, physically based distributed models do account for physical processes that occur within such complex systems. These numerical models often differ from one to another due to a wide range of assumptions that can be taken into consideration during the study (Teutsch and Sauter, 1998; Kiraly, 1998; Kovács and Souter, 2007; Worthington, 2009; Kaufmann et al., 2010; Abusaada and Sauter, 2013; Doummar et al., 2012; Kordilla et al., 2012; Gabrovšek et al., 2018; Chen and Goldscheider, 2014). Distributed numerical models are often used in porous and/or fractured aquifers, however, their application in karstified systems is controversial (Fleury et al., 2007a,b). Karst aquifers can be dominated by secondary (fracture) or tertiary (conduit) porosity that may exhibit hierarchical and complex structures of flow. In addition, turbulent flow components do often occur in such systems. Hauns et al. (2001) provided an explanation for the origin of dispersion and retardation in karst conduits from local scale to catchment scale through numerical simulations and field experiments. The authors suggested that retardation and high dispersion provide evidence of an irregular conduit. Conversely no retardation and moderate dispersion must result from turbulent flow through a smooth conduit. Bodin et al. (2003a,b) described solute transport mechanisms at the fracture scale under natural flow conditions. Other researchers focused on deriving analytical and semi-analytical solutions to describe solute transport mechanisms (Weill et al., 2011; Roubinet et al., 2012; Kumar and Dalal, 2014; Padin, 2016) from experimental and theoretical study of water and solute transport mechanisms conducted in organic-rich carbonate mud rocks. More recently, Deleu et al. (2021) performed a multi-point tracer test across a mapped karstic river section and provided insight into the lateral and vertical heterogeneities in tracer distribution and breakthrough curve shapes. The authors also showed the relevance of probe positioning for a better assessment of spatial heterogeneity of tracer concentration. Gill et al. (2020) compared the performance of semi-distributed and distributed models to simulated karst systems. Authors mentioned that the conductance (conduit diameter) has a big effect on spring discharge, and, semi-distributed models may lack in assessing diffuse contaminant transport in karst aquifers. Moreover, Duran and Gill (2021) modelled a spring flow of an Irish catchment and they showed that conduit geometry and diameter play a big role on controlling spring hydrodynamics of a karstified aquifer.

The main objective of this study is to show the importance of conduit geometry and morphology in controlling flow and solute transport in saturated karst hydrosystems. The study consists of the following steps: (i) 3D mapping of the fully water-filled karst conduit which outlet is the Lez spring, southern France, to get a precise geometry and morphology of the karst conduit; ii) tracer test in real flow conditions, while injecting a dye in the karst conduit and monitoring the the tracer's concentration downstream, at 15 locations and three different cross-sections. In each cross-section, five submersible fluorometer probes were positioned at different locations: top, right, down, left and central parts; and (iii) Modelling solute transport for different geometries and morphologies of the water-filled karst conduit (simplified karst conduit and 3D mapped karst conduit) in order to better assess the sensitivity of flow and transport processes to these properties, while comparing and analyzing simulated and observed BTCs.

2. Field campaign and data acquisition

2.1. Lez spring, southern France

The Lez karst system is characterized by one main outlet, the Lez spring, and several seasonal springs (Fig. 1.a). The Lez spring is located on a tectonic contact (normal fault) striking NE–SW. This vauclusian spring discharges into a pool which overflow is at +65 m above sea level (Fig. 1.b) and feeds the Lez River. The terminal karst conduit of Lez spring (Fig. 1.c) is characterized by a long main conduit of several meters in diameter that makes it accessible by speleological divers. The boundaries of the hydrogeological basin are not precisely known but the area was estimated to be about 250 km^2. Within this hydrogeological basin, there are different recharge zones depending on the nature of the geological cover. Jurassic and Upper Cretaceous limestones occupy an area of between 80 and 100 km^2 and constitute the sectors where most of the recharge of the karst aquifer occurs. The existing boreholes showed that the main conduits network notably developed on the interface between the Cretaceous and Jurassic, limestone formations (Dausse et al., 2019). The Lez Spring is tapped to supply water to the city of Montpellier, located about 10 km downstream. The management of the Lez aquifer consists in pumping water directly within the karst conduit at a depth under the level of the karst spring outlet (Avias, 1995; Jourde et al., 2014). Therefore, the water level can drop below the overflow level of the spring during low-flow conditions, when the

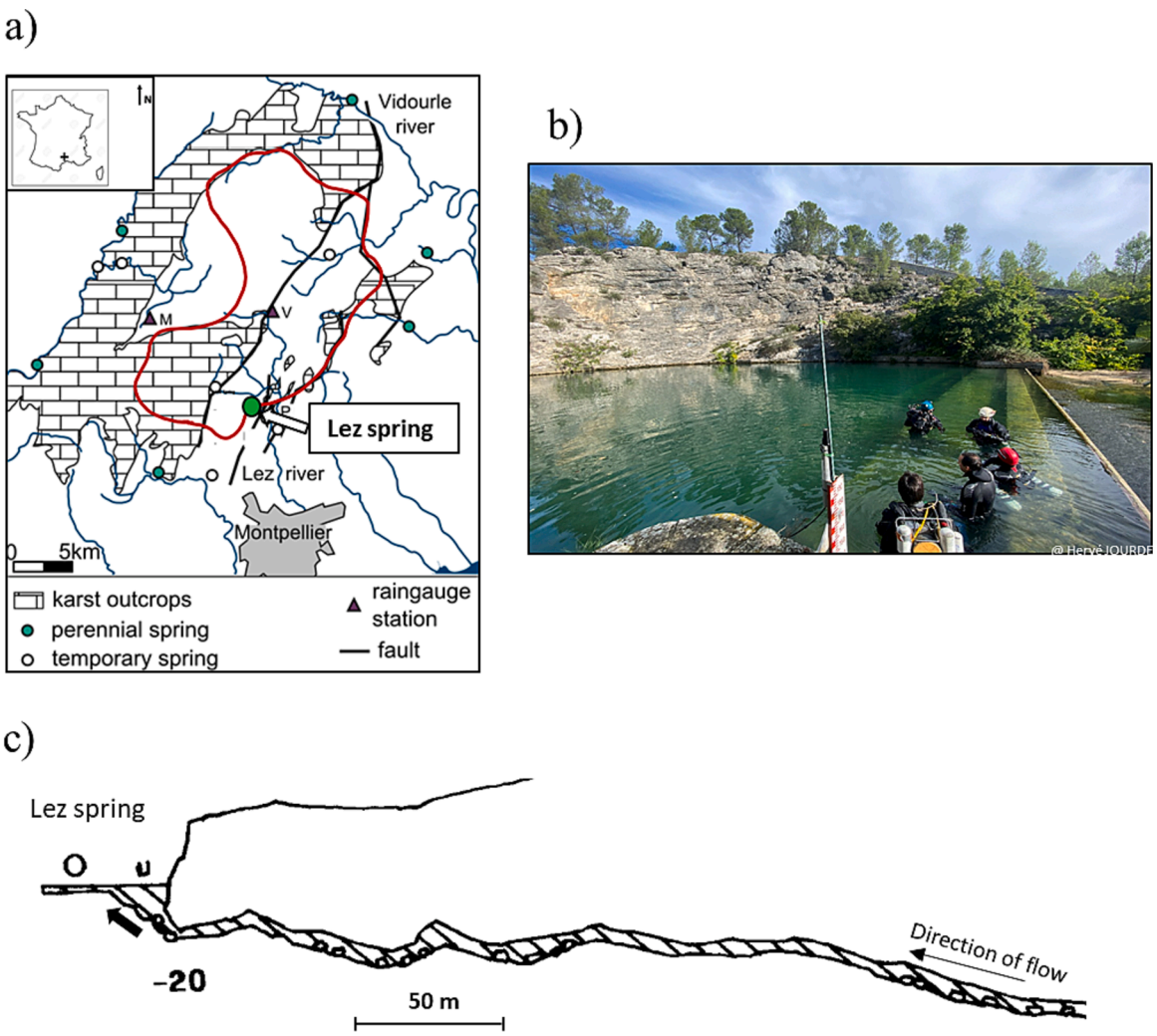

Fig. 1. a) Hydrogeological map and boundaries (in red) of the hydrogeological basin related to the Lez spring karst (Southern France.), modified from (Mazzilli, 2011; Léonardi et al., 2013) Water level at the Lez spring pool (November 2022) when tracer tests were performed (photo by Hervé Jourde).). c) Sketch of the Lez spring terminal conduit geometry in the first 250 m (Original topography by P. Rousset, G.E.P.S diving group, 1972). (For interpretation of the references to color in this figure legend, the reader is referred to the web version of this article.)

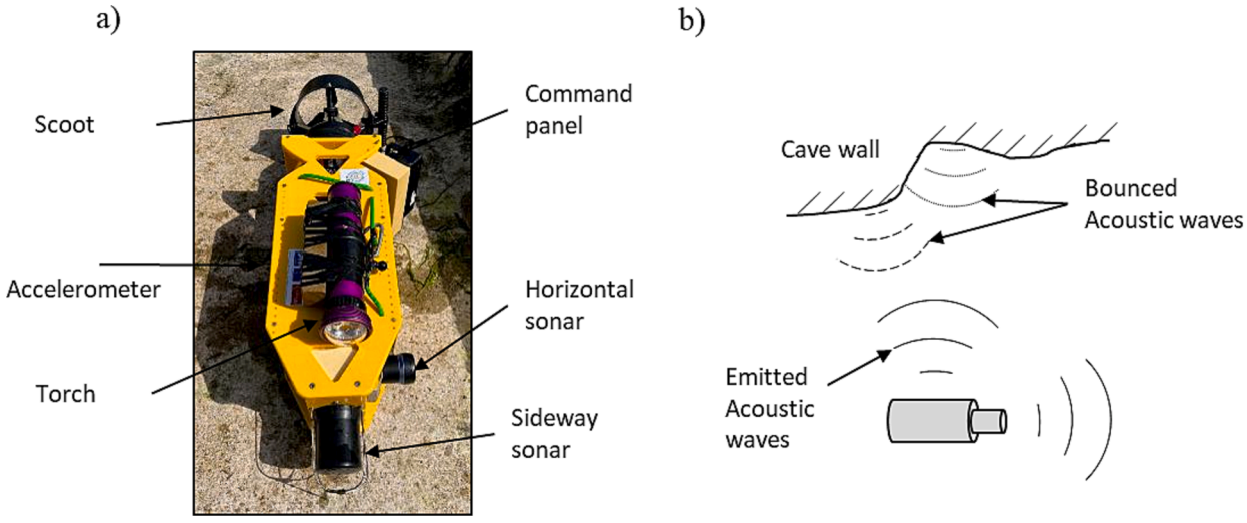

Fig. 2. (3D mapping submersible tool used in this study. a) Picture of the tool coupled with an underwater scooter and a torch. b) a simplified scheme showing how the tool maps the cave using frontal and sideway sonars.

pumping rate exceeds the natural discharge of the karst aquifer. Thus, when the water level at the pool is under 65 m ASL, there is no overflow. The mean annual pumped groundwater extraction is about 1 m^3/s, though groundwater pumping varies daily and seasonally according to the city's needs. Nevertheless, the experiments in this study were performed under pseudo steady state flow condition with no change in the overflow, neither in the discharge at the spring.

2.2. Three dimensional mapping of the terminal karst conduit

Karst conduit's geometry and morphology are usually hard to characterize. In this study, we focus on the Lez spring terminal karst conduit that is accessible by speleological divers. We used a submersible mapping tool (see Fig. 2.a) developed by REEDS® that mainly consist of sonars and accelerometers which allow to reconstruct the three-dimensional geometry and morphology of the studied system. The mapping tool system is carrying a complete sensor's suite to reconstruct system's trajectory (Doppler Velocity Log, DVL1000 @Nortek – and Inertial Central Unit - Ellipse D @SBG) and samples environment with two profiling sonars (Vertical Profiling Sonar -SeaKing @Tritech, Horizontal Profiling Sonar - Ping 360 @BlueRobotics). This tool emits directional acoustic waves while cruising. Part of the acoustic waves are bounced from cave walls and are sent back to the tool that continuously monitor them (Fig. 2.b). Then, the propagation time of the different acoustic waves are interpreted into wall distances which allows to reconstruct a three-dimensional cave map. Meanwhile, the accelerometers of this tool allow to detect the bends of the mapping tool system during the cruise.

Fig. 3 shows the 3D map of the water filled karst conduit obtained with the cave mapping tool. This 3D map is obtained after processing the raw data and slightly smoothing the cave walls.

The karst conduit which outlet is the Lez spring consists mainly on one single conduit with no noticeable branches. It is clearly very tortuous horizontally and vertically. At some locations, the conduit opens up to a large space that can be defined as a cavity. In general, the diameter of conduit turns around few meters (2–8 m), however, the large observed cavities show diameters in the order of tens of meters (10–25 m).

2.3. Tracer test in the water-filled karst conduit

This study is the result of different subaquatic explorations. Firstly, we identified the most relevant part of the conduit to perform the tracer test; the chosen part is quasi rectilinear with no branches. Within this part of the conduit, an injection and three monitoring cross-sections located at distances of 40 m, 90 m and 160 m downstream the injection location were fixed (Fig. 4.a), each cross-section comprising 5 submersible fluorometer probes located in the top, right, down, left and central parts of the conduit cross-section (Fig. 4.c) to allow the reconstruction of the transient dye plume passing through. For the dye injection in the fully water filled karst conduit, we designed a tool called TRACI (Fig. 4.b) that was assembled at REEDS. The dye injection tool consists in a pocket filled with dye solution linked to a submersible pump which is controlled by a chip that takes the activation time and duration of injection as inputs (the delayed dye injection gives the speleological divers time to exit the karst conduit). The peristaltic pump located within the TRACI thus allows to inject dye during 30 s as a step injection signal.

Then, we performed two different tracer tests by injecting a specific amount of dye (Uranine) in the karst conduit at the injection location (Fig. 4). During the tracer tests, the Montpellier water management authority reduced pumping rate so that the outflow at the spring is kept relatively constant (Fig. 5.a). The mean discharge of the spring during the two tracer tests was 390 l/s during tracer test 1 and 410 l/s during tracer test 2.

Fig. 5 shows a compilation of the two tracer tests results. Fig. 5.a

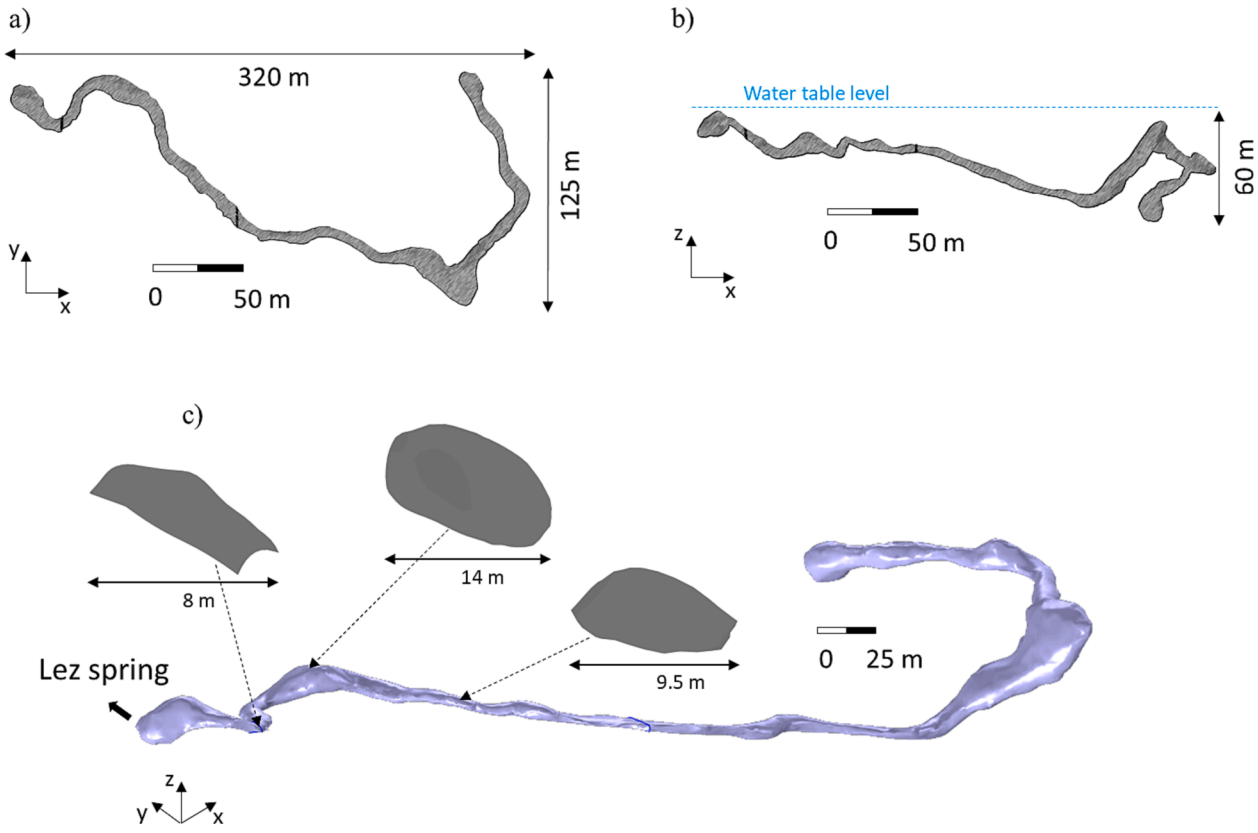

Fig. 3. Mapped of the karst conduit which outlet is the Lez spring. a) Map view. b) Vertical cross section. c) 3D rendering of the mapped karst conduit.

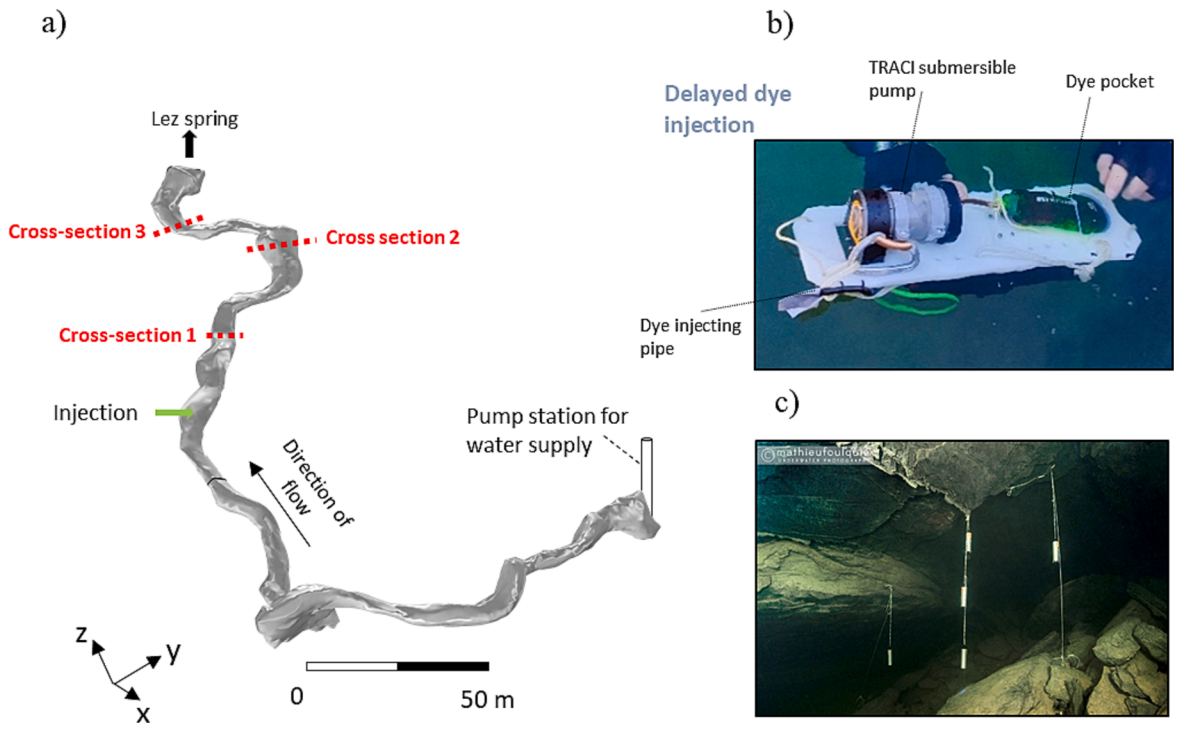

Fig. 4. Tracer test setup. a) Render of the 3D mapped conduit showing the location of injection and monitoring cross-sections. b) TRACI, submersible tool for delayed dye injection. c) Spatial distribution of monitoring probes in cross-section 3 (photo by Mathieu Foulquié).

represents a plot of spring discharge during the tracer tests. The two injection times are highlighted by a green arrow and the monitoring time windows by red intervals (each monitoring window is equivalent to 6 h). The spring discharge variations observed in between the tracer tests are due to pumping rates variations at the pumping station. The concentration of the injected dye, amount of injected dye and mean spring discharge are slightly different between the two tests; the values are summarized in Fig. 5.b and 5.c. Fig. 5.b shows the 15 observed breakthrough curves monitored by the 15 submersible fluorometer probes during tracer test 1. The origin of time axis corresponds to the exact injection time of the dye, and three distinct groups of curves corresponding to the three different monitoring cross-sections clearly appear; cross-section 1 (solid lines) which is the closest to the injection point, cross-section 2 (dashed lines) which is in the middle, and cross-section 3 (dotted lines) which the furthest from the injection point. The comparison between the three groups of curves clearly shows the effect of dye dispersion; the farther is the monitoring cross-section from the injection point, the lower is the peak concentration value and the higher is the longitudinal spread of the dye plume (and lower are the fluctuations). Cross-section 1, which is the closest to the injection point (40 m away from injection point), shows a high degree of fluctuation that can be caused by the bad mixing of the dye in water before this cross-section. Cross-section 2, which is in the middle (90 m away from injection point), exhibits much less fluctuations, that yet remain visible. Cross-section 3, which is the furthest to the injection point (160 m away from injection point), is characterized by negligible fluctuation. Results show that increasing the distance from the injection point leads into a more distributed dye concentration plume across the conduit section. Also, measurements become gradually less heterogeneous along the conduit which might be the result of gradual mixing of the dye in the conduit. Fig. 5.c is a compilation of the observed breakthrough curves of dye concentration for tracer test 2 as a function of time. In general, the results of tracer test 2 show a similar behavior as observed in the results of tracer test 1 (peak concentration value, recession and fluctuations). However, differences can be noticed especially in the restitution curve of dye concentration monitored in cross-section 1 where the BTCs measured by fluorometers seem very different between the two tests. For instance, for tracer test 1, the dye concentration monitored in 1l (Left side of the conduit, red color) shows higher values than in 1R (right side of the conduit, green color). Conversely, for tracer test 2, dye concentration in 1l is lower than dye concentrations in 1R. Such differences might be the result of either the slightly higher discharge for tracer test 2 than for tracer test 1 or complex flow circulation that changes over time. Besides, the bad mixing of the dye combined with localized flux turbulences might explain both the fluctuations and these differences between tracer tests 1 and 2 observed in cross-section 1. These assumptions will be tested in the "numerical modelling" section.

3. Three dimensional modelling of flow and solute transport

3.1. Governing equations

3D flow simulations considering the geometry and morphology of the conduit are setup and performed using the COMSOL Multiphysics software. The different numerical simulations of this study account for laminar and/or turbulent flows within conduits in steady state condition. Then, the steady state flow solution is considered to simulate transient solute transport. The model uses a finite tetrahedral elements mesh and an adaptive time stepping with a maximum time step of $\Delta t = 10$ s. Hereafter, we summarize the main flow and transport equations that are taken into considerations as well as the main assumptions. The governing statement for flow in the conduit comes from the Navier-Stokes equations, which combine a momentum balance with an equation of continuity. The Navier-Stokes equations solve velocity and pressure for dependent variables. The simplification of the Navier-Stokes equations solved in this study are the Reynolds-Averaged Navier–Stokes (RANS) equations for conservation of momentum, the continuity equation for conservation of mass, and an algebraic turbulence model. The algebraic yPlus turbulence model, used here, is based on the distance to the nearest wall. The model is based on Prandtl's mixing-length theory for wall-bounded turbulent flows. Thus, the turbulence eddy viscosity is a function of scaled wall distance. In this case,

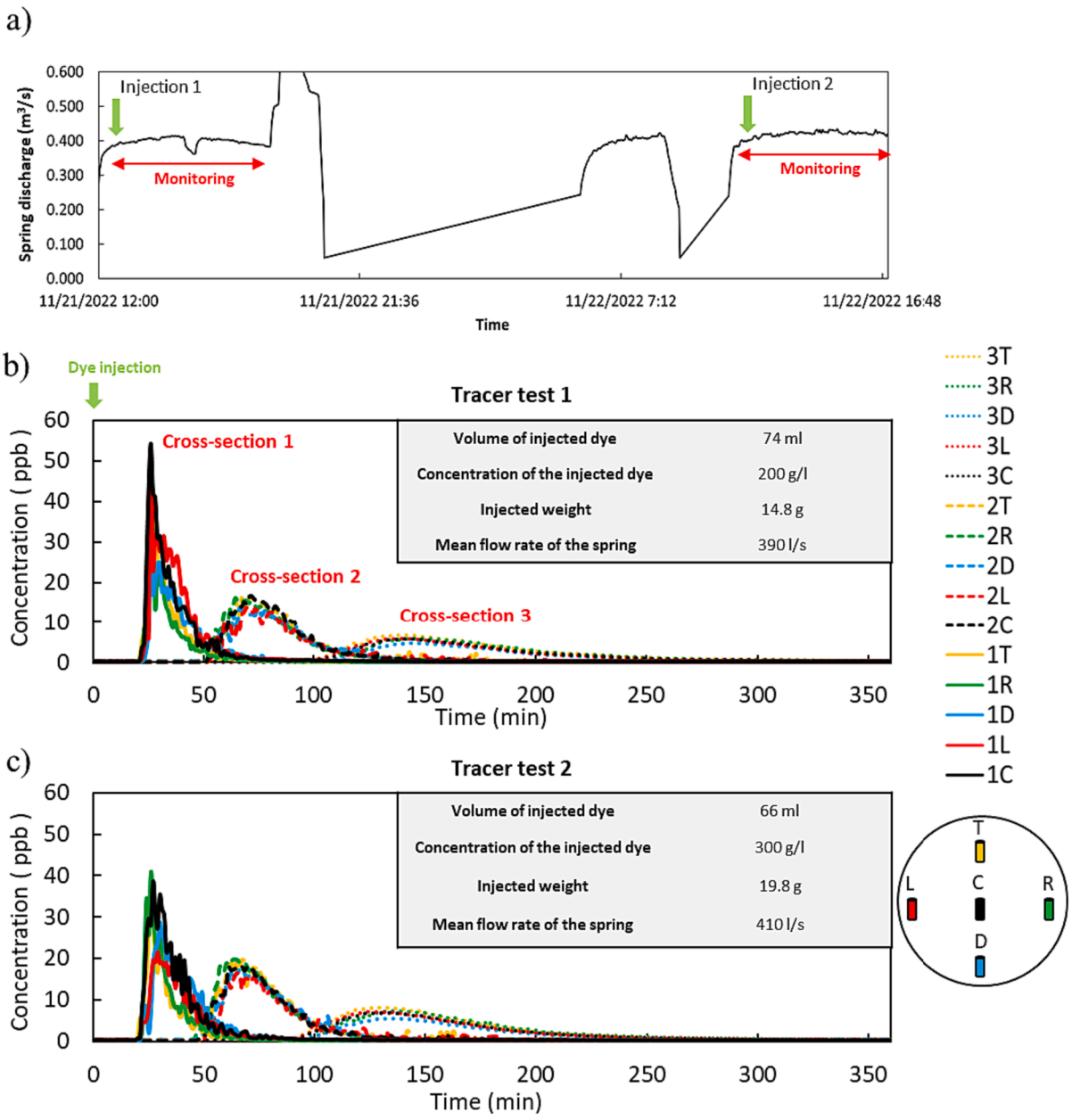

Fig. 5. Results of the tracer test performed in the water filled karst conduit. a) Lez spring discharge during the experiment corresponding to the two monitoring windows. b) Breakthrough curves at the three monitoring cross-sections during tracer test 1; each cross-section comprises 5 probes (T → Top, R → Right, D → Down, L → Left and C → Central, left and right are represented looking downstream). c) Breakthrough curves at the three monitoring cross-sections during tracer test 2, for the same monitoring configuration as during tracer test 1.

the fluid (water) has constant density and viscosity. Equation (1) is the momentum equation and Eq. (2) is the conservation of mass.

$$\rho(u\nabla)u = -\nabla p + \frac{1}{Re}\nabla^2 u + \rho g \tag{1}$$

$$\rho\nabla u = 0 \tag{2}$$

with the boundary conditions

$$v_{inlet} = cst \tag{3}$$

$$p_{outlet} = p_{atm} \tag{4}$$

where u is the velocity, p is the pressure, ρ is the fluid density, g is the gravity, Re is the flow Reynolds number. v_{inlet} is the uniform velocity at the conduit inlet. p_{outlet} is the pressure at the conduit outlet. p_{atm} refers to the atmospheric pressure.

Concentration field of a diluted solute in water is then numerically estimated. The driving forces for transport are diffusion solved with Fick's law and convection using the flow field previously solved with the RANS equations. The governing equation can be written as follow:

$$\frac{\partial c}{\partial t} + \nabla(D\nabla c) + u\nabla c = 0 \tag{5}$$

where c is the molar concentration of a diluted solute in water, D is the diffusion coefficient and u is the flow velocity field. The tracer is injected as a Gaussian pulse during the first 30 s of the simulation using a point injection boundary condition.

3.2. Observed versus simulated tracer test

In this section, tracer test 1 is considered and the BTCs simulated at the 15 measurements location are compared to observed BTCs, while considering two karst conduit geometries. The first karst conduit case, referred to as "simplified geometry" is built with spheres and cones with smooth surfaces. This geometry is based on former mapping of the karst conduit (classical map view and cross section), performed by speleological divers in the 1970's. The second karst conduit geometry is built on the basis of data gathered by the 3D mapping submersible tool and is referred to as "3D mapped geometry". For both geometries, steady state flow modelling is realized for the discharge measured during tracer test 1 (390 l/s), then solute transport simulation is performed. Simulations results obtained for the simplified and 3D mapped geometries were then compared to get insights about the effect of an accurate geometry and morphology on flow and transport processes in the water filled karst conduit. For all simulations, t = 0 corresponds to the injection time of the dye.

Fig. 6.a shows the BTCs at the 15 location points and in the 3 cross-sections obtained for the simplified geometry.: cross-section 1 (solid lines) which is the closest to the injection point, cross-section 2 (dashed lines) which is in the middle, and cross-section 3 (dotted lines) which is

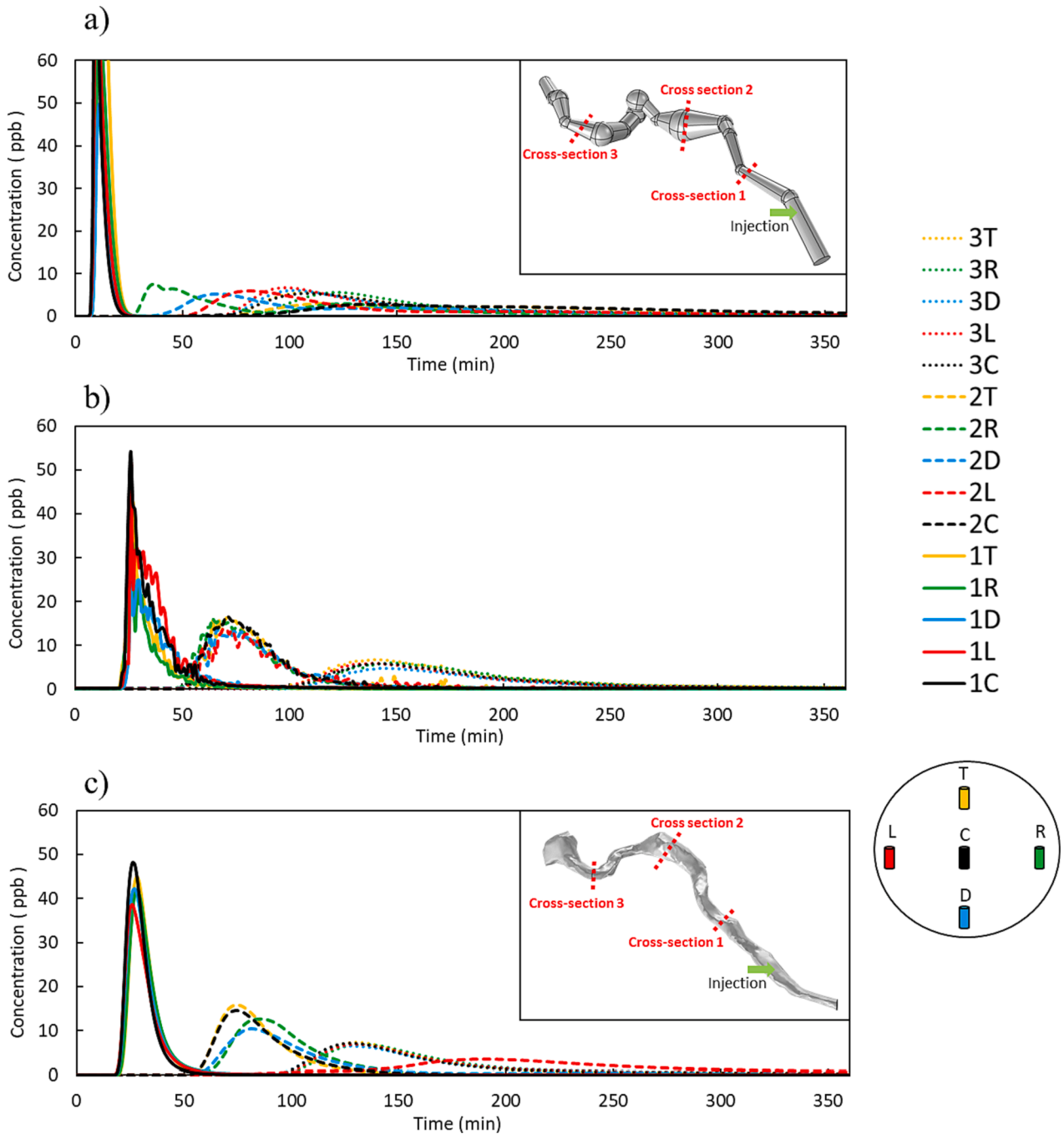

Fig. 6. Results of simulated tracer tests using the simplified geometry and the 3D mapped geometry of the karst conduit at the three monitoring cross-sections.; each cross-section has five monitoring locations (T → Top, R → Right, D → Down, L → Left and C → Central, left and right are represented looking downstream). a) Simulated BTCs for the simplified geometry b) Observed BTCs for tracer test 1 measured at the three monitoring cross-sections in a similar monitoring configuration. c) Simulated BTCs for the 3D mapped geometry.

the furthest from the injection point.

Simulation results obtained for the simplified geometry (Fig. 6.a) clearly exhibit a different transport behavior than the one observed during the tracer test (Fig. 6.b), as highlighted by the different first arrival times and values of dye concentration. Fig. 6.c shows the simulated BTCs obtained at each monitoring point, while considering the 3D mapped conduit geometry. Simulated first arrival times and peak concentration values for the different cross-sections are in agreement with observed data (Fig. 6.b), which means that the consideration of the true geometry and morphology of the water-filled karst conduit significantly improves the modelling results at local scale.

Mapping both geometry and morphology of the karst conduit is thus important to correctly simulate the 3D spatial and temporal dispersion of the dye. Accordingly, the knowledge of the general geometry of the karst conduit is insufficient to properly predict solute transport and dye plume propagation.

Nevertheless, some observations are not properly reproduced. Both simulations do not capture the fluctuations of dye concentration that can be observed especially for cross-section 1 (Fig. 6.b). It might be due to complex mixing processes that are not captured with the numerical simulation. Furthermore, even for the most satisfying simulation obtained with the 3D mapped geometry, some differences can be observed in cross-section 2 at location 2l, where the simulated BTC is significantly delayed with respect to the observed BTC.

To better assess the origin of the differences between observed and simulated results obtained with the 3D mapped geometry, we looked at the simulated concentration along the cross section of the conduit in cross-section 2. Fig. 7.a shows the simulated concentration in cross-section 2 at the peak concentration time (t = 75 min). It shows that the dye plume is localized in the right side of the conduit. In this cross-section, the size of the conduit (Fig. 7.a) is large (about 15 m width and 10 m high). For such large dimension, the precise location of the probes is challenging for speleological divers. Moreover, the submersible mapping tool can induce measurements errors when mapping deep and narrow lateral voids. For example, along a bedding plane where the conduit is horizontally lens-shaped (Filipponi et al., 2010), the mapping tool tend to underestimate the horizontal diameter (see Fig. 7.c). Fig. 7.b shows simulated BTCs in cross-section 2 for two slightly different locations of the monitoring probes represented by white (solid lines) and black (dashed lines) dots (Fig. 7.a). Based on the simulated BTCs obtained for the two different monitoring configurations, the delay of simulated BTC in 2l could be explained by a small bias in the measurement location combined with a highly heterogeneous plume. According to these results, a very precise location of the monitoring probe is thus required to properly reproduce transport processes in the water filled karst conduit. Even though five probes were used per cross section during the tracer test, some cross-sections may require further monitoring points in order to better capture the spatial distribution of the concentration in the dye plume.

We also initiated an investigation about the observed differences between the tracer tests 1 and 2 for cross-section 1. Firstly, results showed that using $Q_2 = 410$ l/s instead of $Q_1 = 390$ l/s doesn't change the BTCs in cross-section 1 as observed in real data; the velocity profile remained similar and the velocity values were slightly higher. Thus, the bad mixing of the dye combined with localized flux turbulences might explain both the fluctuations and these differences between tracer tests 1

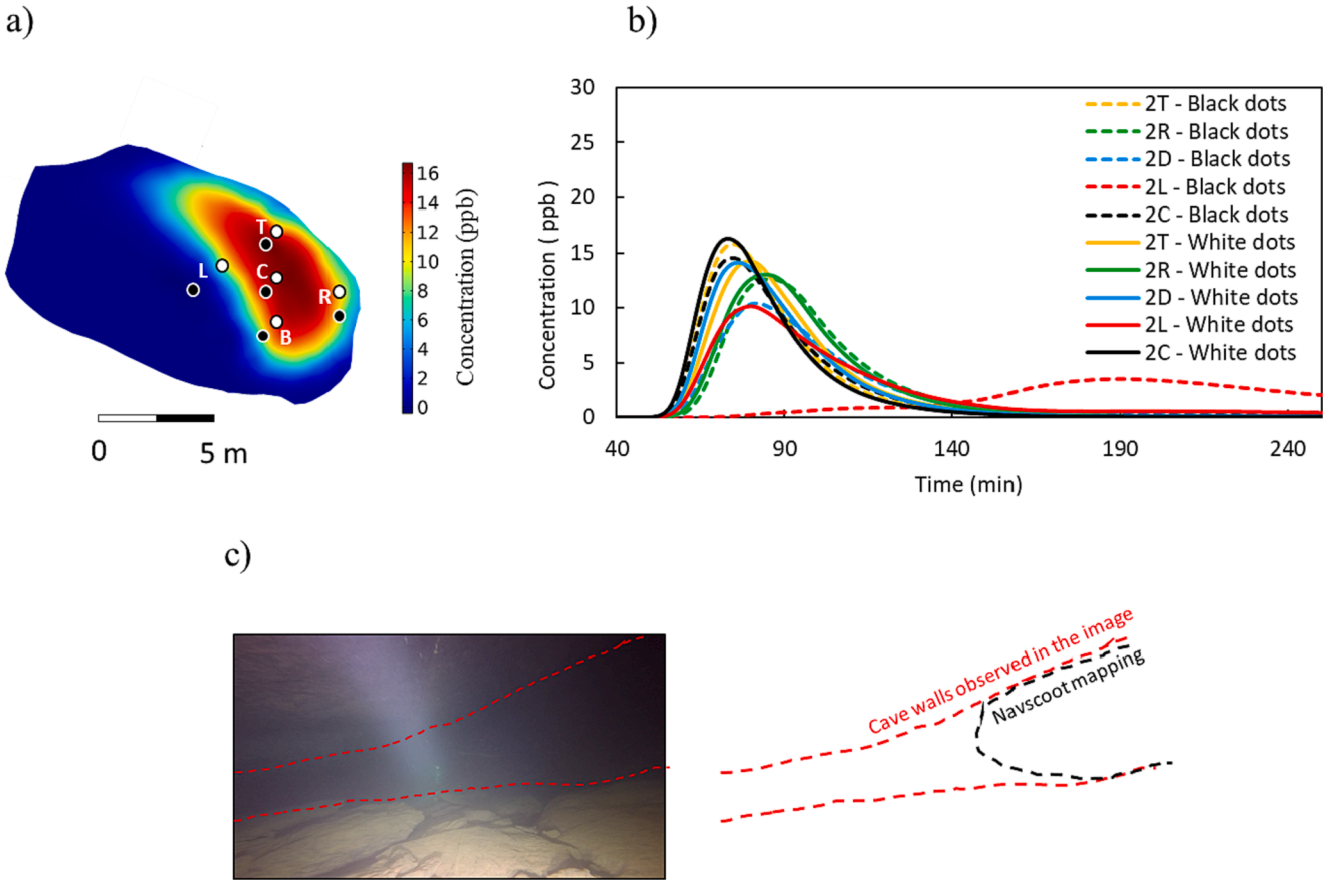

Fig. 7. Results of simulated tracer test 1 in cross-section 2 for the 3D mapped geometry. a) Concentration profile across cross-section 2 at peak time (t = 75 min). b) Simulated BTCs at the five monitoring locations (T → Top, R → Right, D → Down, L → Left and C → Central, left and right are represented looking downstream) in cross-section 2, considering different measurements locations (black dots for dashed lines and white dots for solid lines). c) Example of a mapping error where the mapping tool can lead to an underestimation of the horizontal dimension in a lens-shaped conduit.

and 2 observed in cross-section 1.

3.3. Synthetic tests in simple karst conduit geometries

In order to better understand the effect of conduit geometry and morphology on flow and solute transport, we here focused on simulating tracer tests for different karst conduit cases and our reference case consists in a straight conduit (100 m length and 5 m diameter). We refer to conduit geometry as the general backbone structure of the conduit (linearity, tortuosity, bends, …) and to conduit morphology as the shape of the conduit wall and diameter variations. Fig. 8 shows three different cases that feature heterogeneities in conduit geometry and morphology (i.e. bend and wall asperity). Next to each case, a plot of a two dimensional velocity profile (map view) obtained in steady state regime is provided. For these cases, a similar setup as the one considered for the tracer test is considered and the simulated concentration is assessed in a given monitoring cross-section at five measurement locations (Fig. 8). For the different simulations, the total length of the conduit is the same (100 m). The steady state flow is first simulated with a constant flow rate of Q = 390 l/s. Then, solute transport simulation is performed after injecting 74 ml of dye with a concentration of 200 g/l 20 m downstream from the flow inlet (green arrow) which corresponds to 14.8 g of injected dye. The monitoring cross-section is located 80 m downstream from the inlet.

The first case, referred to as "Uniform conduit", consists of a straight cylindrical conduit with a constant diameter of 5 m (Fig. 8.a). The second case, referred to as "Curved conduit", consists of a cylindrical conduit with a 90° bend in the middle (Fig. 8.b). The bending conduits turns right and its diameter is also 5 m. The third case, referred to as "Non-Uniform conduit", is a straight conduit formed with the same characteristics as the uniform conduit, with 3 spheres (8 m diameter) in the middle (Fig. 8.c). Thus, the first case corresponds to a basic configuration. The second case is considered to highlight the effect on 3D flow and solute transport of a change in geometry while the third case is considered to highlight a change in morphology (wall asperity/diameter). Velocity profile for the three different cases (Fig. 8) already shows how geometry and morphology affect hydrodynamics. For the first case (Uniform conduit), a uniform parabolic velocity profile is observed along the whole conduit. For the second case (Curved conduit), the same parabolic velocity profile is observed before the bend, but significantly changes beyond the bend: flow focused in the right side of the conduit at the bend and in the left side of the conduit after the bend. For the third case (Non-Uniform conduit), an almost parabolic velocity profile is observed, which however is slightly modified by the changes in conduit diameter (see zoomed profile in Fig. 8.c).

Fig. 9 shows the simulated BTCs at the five locations of the monitoring cross-section. Fig. 9.a shows the simulated BTCs obtained for the "Uniform conduit" (solid lines) and the "Curved conduit" (dashed lines), respectively. Fig. 9.b shows the BTCs obtained for the "Uniform conduit" (solid lines) and the "Non-Uniform conduit" (dashed lines), respectively. For the "Uniform conduit" case, the simulated dye concentration is higher in the center than at the four other measurements locations near the conduit walls. It also shows a quicker dye breakthrough in the center, which can be explained by the parabolic flow velocity profile.

The "Curved conduit" case shows a quicker dye breakthrough than the "Uniform conduit" case. According to this result, conduit tortuosity accelerates dye breakthrough. For the "Curved conduit" case, the highest dye concentration is not obtained in the center of the conduit

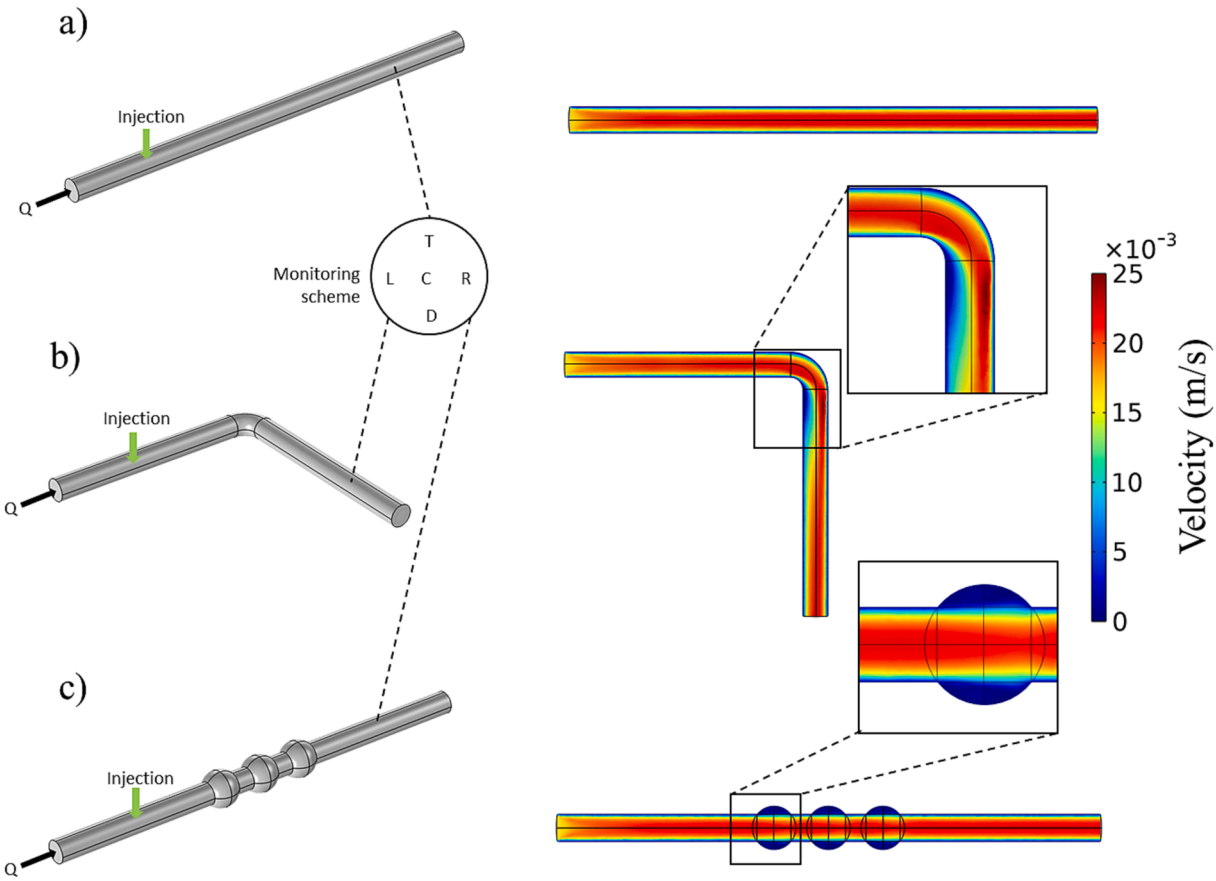

Fig. 8. Simple three-dimensional conduit geometries/morphologies and its corresponding flow velocity profiles under constant flow rate condition (Q = 390 l/s). a) Uniform and linear conduit. b) Curved conduit with uniform diameter. c) Non-uniform (variable diameter) linear conduit (T → Top, R → Right, D → Down, L → Left and C → Central, left and right are represented looking downstream).

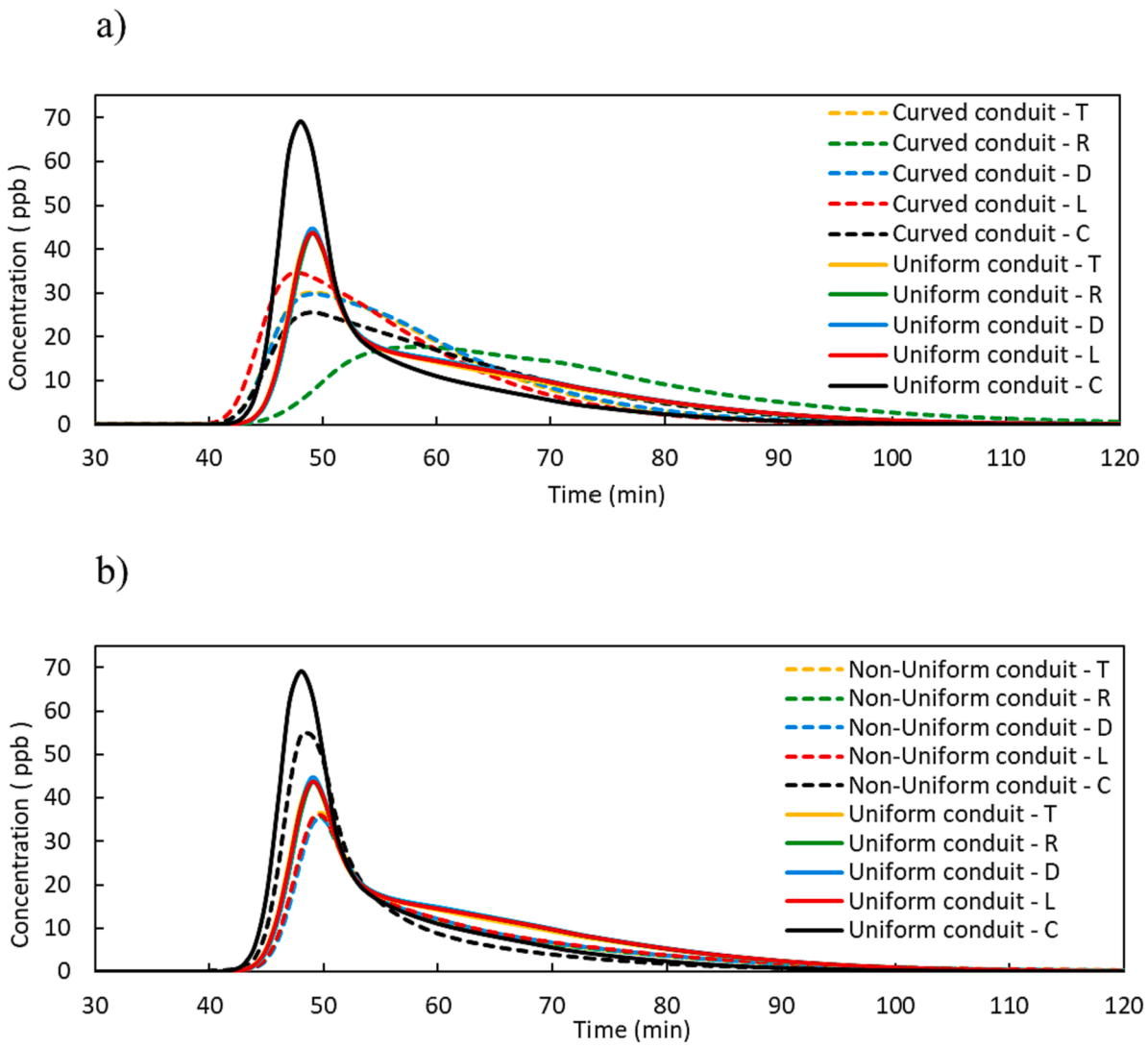

Fig. 9. Results of a simulated tracer test within the simple three-dimensional conduit geometries a) BTCs of concentration measured at the five monitoring locations (T → Top, R → Right, D → Down, L → Left and C → Central, left and right are represented looking downstream) for the uniform and curved conduit cases. b) BTCs of concentration measured at the same five monitoring locations for the uniform (solid lines) and non-uniform (dashed lines) conduit cases.

anymore but at the location L (left side of the conduit; the bend is toward the right). Also, much lower value of dye concentration and a delayed first arrival time is observed at location R (right side of the conduit). For the "Curved conduit" case, there is a higher dispersion of the dye plume than the one observed for the "Uniform conduit" case.

The "Non-Uniform conduit" case shows a slightly slower dye breakthrough than the "Uniform conduit" case. This result can be explained by the changes in conduit asperity/diameter that generates slower flow velocities, and hence the slightly delayed BTC. For both cases, the highest dye concentration is obtained in the center of the conduit while lower dye concentrations are observed near the conduit walls. Though the dispersion is relatively similar for both geometries, the changes in conduit diameter/asperity induce lower peak concentration values as well as longer tailing.

According to results shown in Fig. 9, the "Curved conduit" case generates lower peak concentrations values, smaller breakthrough time and higher dispersion of the dye plume than the two other conduit's geometries. Meanwhile, the "Non-Uniform conduit" case generates slightly lower peak concentrations and slower breakthrough time than the one observed for the "Uniform conduit" case, whilst the dispersion of the dye plume dispersion remains similar for both geometries.

A last case, referred to as "Curved – Non Uniform conduit" case, combining a right bend and conduit diameter variations, has been considered (Fig. 10.a). 3D flow and solute transport simulation were performed with the same boundary conditions as for the previous cases. Fig. 10.b shows a two dimensional map view of flow velocity profile for this case. A higher alteration of the standard parabolic velocity profile can be observed and rapid flow near the conduit walls occurs more often than for the previous geometries. Fig. 10.c shows the simulated BTCs obtained for the "Curved - Uniform conduit" case (solid lines) and the "Curved - Non Uniform conduit" case (dashed lines), respectively. The "Curved - Non Uniform conduit" case generates a delayed breakthrough time, a lower peak concentration value and a different dispersion of the dye plume than the one observed for the "Curved – Uniform conduit" case. As the right bend in the middle part of the conduit is the same for both cases, we would expect a similar influence of diameter variations on solute transport processes but a more significant dye plume alteration is observed for the "Curved – Non Uniform conduit" case. This case highlights the effect of both morphological and geometrical heterogeneities on transport processes. Moreover, both "Curved – Uniform conduit" and "Curved – Non Uniform conduit" geometries show quicker dye breakthrough in the left side and slower dye breakthrough in the right side. Such result is caused by the right bend.

Fig. 11 shows velocity and concentration profiles for the four

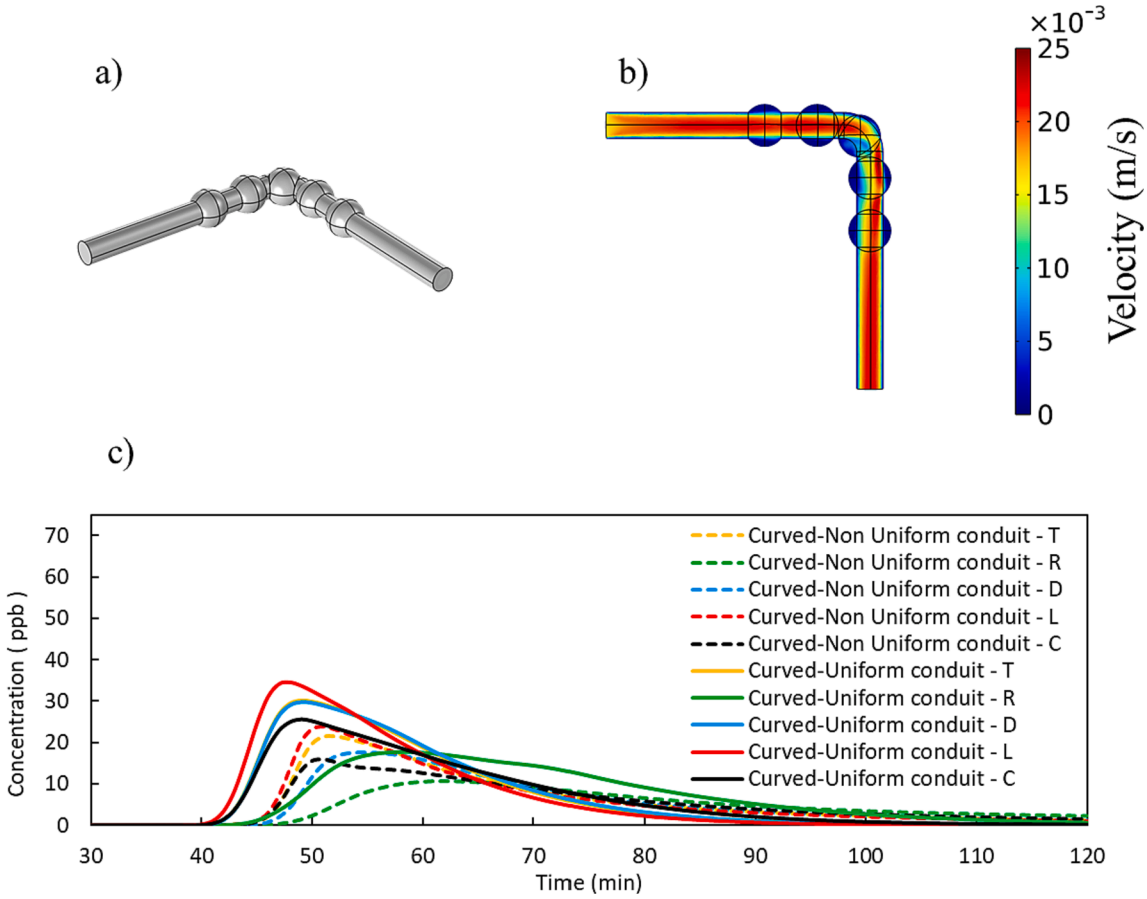

Fig. 10. Results of a simulated tracer test within the simple three-dimensional conduit geometries. a) Curved conduit with non-uniform diameter. b) Corresponding flow velocity profile under constant flow rate condition. c) Simulated BTCs of concentration measured at five monitoring locations (T → Top, R → Right, D → Down, L → Left and C → Central, left and right are represented looking downstream) for the curved-uniform (solid lines) and curved-non uniform (dashed lines) conduit cases.

different synthetic cases at the monitoring cross-section during peak concentration: "Uniform conduit" case (Fig. 11.a), "Non-Uniform conduit" case (Fig. 11.b), "Curved Uniform conduit" case (Fig. 11.c) and "Curved Non-Uniform conduit" case (Fig. 11.d). Results show different transport behaviors for the different cases. The existence of bends in karst conduits alters the velocity profiles which induces dye transport near the walls (Fig. 11.c and d). The existence of asperity/diameter variations in addition to bends of the karst conduits can temporarily trap the dye and create inertial flow loops that delay the dye breakthrough and lower peak concentration values (Fig. 11.b and d). According to these results, not only conduit geometry can affect solute transport but conduit morphology (i.e. asperity/diameter variation) can also significantly modify the general behavior of transport (flow recirculation, increased turbulence).

These synthetic simulations allow to assess the effect of simple heterogeneities in geometry and morphology on 3D flow and transport processes, which should provide guidance for more in-depth analyses of the real tracer tests data. For instance, the cross-section 1 in Fig. 5 is located after a relatively straight conduit. Simulations in such configuration state that dye concentration is higher in the center and lower near the conduit walls. Fig. 5.b and 5.c, that correspond respectively to the results of tracer tests 1 and 2, show that dye concentration obtained in the central monitoring point (solid black line) is indeed higher. However, it is not as obvious as in synthetic simulations and it is not higher than at all the other monitored locations which are closer to cave walls. According to this results, simulated tracer test BTCs seems to be more heterogeneous than observed BTCs. Moreover, the cross-section 2 is located after a left bend (Fig. 3.a). Simulations in such configuration state that dye breakthrough curve will have a higher peak concentration value and a smaller first arrival time in the right side of the conduit while a lower peak concentration value and a slower first arrival time are expected in the left side. Indeed, we observe that, in cross-section 2 for both tracer tests 1 and 2, dye concentration in the left side (dashed red line) is lower than concentrations at the other monitoring locations (Fig. 5). However, it is not as contrasted as in the simple synthetic cases. Finally, for both tracer tests 1 and 2, breakthrough curves monitored in cross-section 3 show that concentration measured in 3 T → Top location is higher than in 3D → Down location. Based on the synthetic tests, the cross-section 3 is expected to be either in a horizontal conduit preceded by an uprising conduit, or in a downward-sloping conduit. However, the 3D mapped geometry shows that cross-section 3 is located at an uprising conduit and at the beginning of a right turn (Fig. 4.a and 4.c). We also notice that, most of the time, the concentration in the top part of the conduit is higher than the concentration in the bottom part of the conduit. Such results might state that the dye plume and/or the velocity profile are slightly decentralized upwards. As the density effects are negligible for the dye concentration injected during the tracer tests, this results might be caused by the superimposed effect of different heterogeneities along the water-filled karst conduit (several bends and wall asperity).

4. Summary and conclusions

In this study, the Lez terminal karst conduit was mapped to get the precise geometry and morphology of this fully water-filled karst conduit. Then, a tracer test in the water-filled karst conduit was performed for

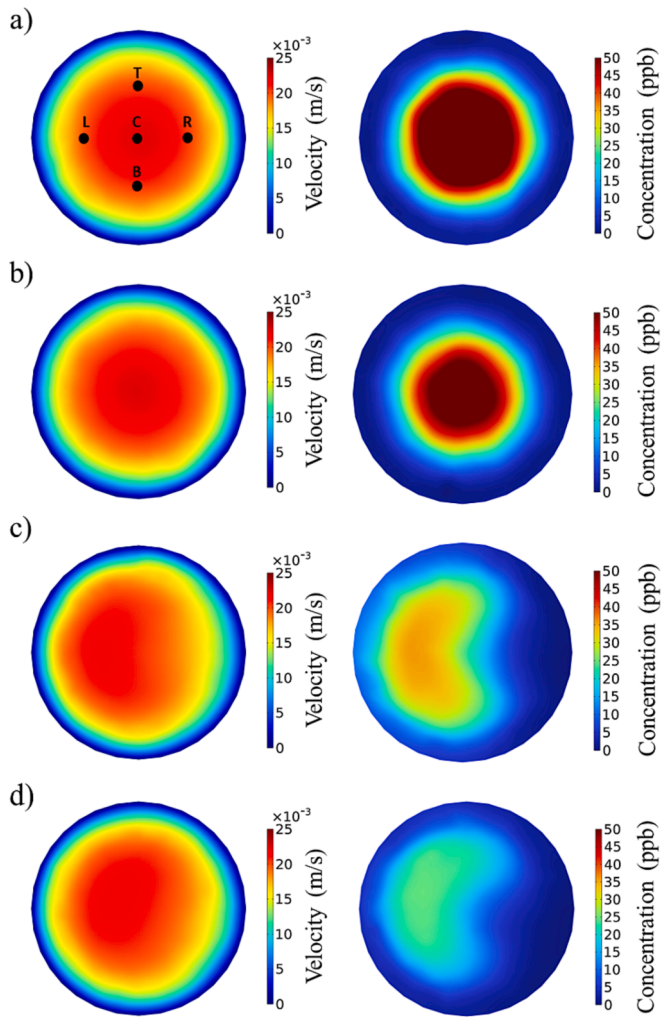

Fig. 11. Velocity and concentration profiles for the different synthetic cases at the monitoring cross-section during peak concentration. a) Uniform and linear conduit. b) Non-uniform (variable diameter) linear conduit. c) Curved conduit with uniform diameter. d) Curved conduit with non-uniform diameter.

real flow conditions; a dye was injected and the concentration was monitored at three different cross-sections of the karst conduit located downstream at distances of 40 m, 90 m and 160 m, respectively. In each cross-section, five submersible fluorometer probes were placed at different locations (top, right, down, left and central parts of the cave) along the cross-section of the karst conduit. Also, numerical simulations were used to reproduce the observed tracer tests data, and, several synthetic cases of tracer tests considering different geometries and morphologies improved the assessment of the hydrodynamics and solute transport mechanisms within the water filled karst conduit.

This study allows to state several conclusions:

- Firstly, results clearly show the effect of dye dispersion; the farther is the monitoring cross-section from the injection point, the lower is the peak concentration value and the higher is the longitudinal spread of the dye plume (and lower are the fluctuations).
- A particular transport behavior is observed in the tracer tests performed in the water filled conduit, as highlighted by the BTCs which exhibit fluctuations in dye concentration that attenuates as the dye plume moves downstream. The bad mixing of the dye combined with localized flux turbulences might explain both the fluctuations and these differences between tracer tests 1 and 2 while the dispersion of the dye can also explain the attenuation of the fluctuations in dye concentration when moving downstream the injection spot.
- Using several submersible fluorometer probes, spatially distributed inside the karst conduit cross sections, allowed to assess the dye plume variations in space and time.
- The simplified conduit geometry and morphology of the karst conduit alone seems to be insufficient to capture 3D flow and transport processes. In contrast, the 3D mapped conduit considerably enhanced the simulations and predictions and allowed to provide satisfactory results. Moreover, simulated tracer test BTCs show more heterogeneous shapes of dye plume than the observed BTCs.
- The positioning of monitoring probes is very important for the measurement of BTCs of concentration in karst conduits. Dye plume can be decentralized by the effect of geometry and morphology to parts near the wall of the conduit. For instance, when the study is limited to using only one probe, its location must be chosen as a function of the neighboring geometry in order to obtain measurements close to the center of the plume.
- The geometry and morphology of karst conduits showed a great importance in controlling conduit hydrodynamics and transport processes: Tortuous conduits have lower peak concentration values, quicker first arrival time and higher dispersion of the dye plume. Indeed, a conduit with a right bend decentralizes the dye plume towards the left part of the conduit. Also, conduits with asperity/diameter variations show lower peak concentration values, slower first arrival time but similar dispersion of the dye plume.
- Moreover, the synthetic simulations showed that the existence of asperity/diameter variations in addition to bends of the karst conduits can temporarily trap the dye and create inertial flow loops that delay the dye breakthrough.

CRediT authorship contribution statement

Mohammed Aliouache: Formal analysis, Software, Writing – original draft, Writing – review & editing, Conceptualization, Investigation, Methodology, Visualization. **Pierre Fischer:** Formal analysis, Software, Writing – review & editing, Conceptualization, Investigation, Methodology. **Pascal Brunet:** Resources, Investigation. **Lionel Lapierre:** Conceptualization, Formal analysis, Funding acquisition, Resources, Writing – review & editing, Investigation, Methodology, Supervision. **Benoit Ropars:** Resources, Investigation. **Frank Vasseur:** Investigation, Resources. **Hervé Jourde:** Conceptualization, Investigation, Methodology, Resources, Supervision, Writing – review & editing.

Declaration of competing interest

The authors declare that they have no known competing financial interests or personal relationships that could have appeared to influence the work reported in this paper.

Data availability

Data will be made available on request.

Acknowledgements

This work was achieved within the framework of the multidisciplinary project LEZ 2020, involving: FSE-Occitanie, Montpellier Méditerranée Métropole, Régie des Eaux, Région Occitanie, Centre National de la Recherche Scientifique – CNRS, Solutions robotisées d'inspection subaquatique – REEDS, Institut d'électronique et des systèmes – IES, Polytech Montpellier, Université de Montpellier, Le Laboratoire d'Informatique, de Robotique et de Microélectronique de Montpellier – LIRMM, HydroSciences Montpellier – HSM, LabEx NUMEV, Institut Montpellierain Alexander Grothendieck – IMAG and Systèmes Electroniques-Robotique Appliquée – SyERA. It is supported by FEDER: "Fonds européen de développement régional" program for research, technological development and innovation under LEZ2020 project.

Appendix A. Supplementary data

Supplementary data to this article can be found online at https://doi.org/10.1016/j.jhydrol.2024.130953.

References

Abusaada, M., Sauter, M., 2013. Studying the flow dynamics of a karst aquifer system with an equivalent porous medium model. Groundwater 51, 641–650. https://doi.org/10.1111/j.1745-6584.2012.01003.x.

Avias, J.V., 1995. Gestion active de l'exsurgence karstique de la source du Lez (Hérault, France) 1957–1994. Hydrogéologie (orléans) 1, 113–127.

Barberá, J.A., Mudarra, M., Andreo, B., De la Torre, B., 2018. Regional-scale analysis of karst underground flow deduced from tracing experiments: examples from carbonate aquifers in Malaga province, southern Spain. Hydrgeol. J. 26 (1), 23–40.

Bodin, J., Delay, F., De Marsily, G., 2003a. Solute transport in a single fracture with negligible matrix permeability: 1. fundamental mechanisms. Hydrgeol. J. 11 (4), 418–433.

Bodin, J., Delay, F., De Marsily, G., 2003b. Solute transport in a single fracture with negligible matrix permeability: 2. mathematical formalism. Hydrgeol. J. 11 (4), 434–454.

Chen, Z., Goldscheider, N., 2014. Modeling spatially and temporally varied hydraulic behavior of a folded karst system with dominant conduit drainage at catchment scale, Hochifen-Gottesacker, Alps. J. Hydrol. 514, 41–52.

Dausse, A., Leonardi, V., Jourde, H., 2019. Hydraulic characterization and identification of flow-bearing structures based on multi-scale investigations applied to the Lez karst aquifer. J. Hydrol.: Reg. Stud. 26, 100627.

Deleu, R., Frazao, S.S., Poulain, A., Rochez, G., Hallet, V., 2021. Tracer dispersion through Karst Conduit: assessment of small-scale heterogeneity by multi-point tracer test and CFD modeling. Hydrology 8 (4), 168. https://doi.org/10.3390/hydrology8040168.

Doummar, J., Sauter, M., Geyer, T., 2012. Simulation of flow processes in a large scale karst system with an integrated catchment model (Mike She)—Identification of relevant parameters influencing spring discharge. J. Hydrol. 426–427, 112–123.

Duran, L., Gill, L.W., 2021. Modeling spring flow of an Irish karst catchment using Modflow-USG with CLN. J. Hydrol. 597, 125971.

Fleury, P., Bakalowicz, M., de Marsily, G., 2007a. Submarine springs and coastal karst aquifers: A review. J. Hydrol. 339 (1–2), 79–92.

Fleury, P., Plagnes, V., Bakalowicz, M., 2007b. Modelling of the functioning of karst aquifers with a reservoir model: Application to Fontaine de Vaucluse (South of France). J. Hydrol. 345, 38–49.

Flury, M., Wai, N.N., 2003. Dyes as tracers for vadose zone hydrology. Rev. Geophys. 41, 1002. https://doi.org/10.1029/2001RG000109, 1.

Ford, D., Williams, P.D., 2007. Karst hydrogeology and Geomorphology. John Wiley & Sons.

Gabrovšek, F., Peric, B., Kaufmann, G., 2018. Hydraulics of epiphreatic flow of a karst aquifer. J. Hydrol. 560, 56–74.

Gill, L.W., Schuler, P., Duran, L., Morrissey, P., Johnston, P.M., 2020. An evaluation of semidistributed-pipe-network and distributed-finite-difference models to simulate karst systems. Hydrgeol. J. 29, 259–279.

Goldscheider, N., 2008. A new quantitative interpretation of the long-tail and plateau-like breakthrough curves from tracer tests in the artesian karst aquifer of Stuttgart, Germany. Hydrgeol. J. 16 (7), 1311–1317.

Goldscheider, N., Drew, D. (Eds.), 2014. Methods in Karst Hydrogeology: IAH: International Contributions to Hydrogeology. CRC Press, p. 26.

Hartmann, A., Goldscheider, N., Wagener, T., Lange, J., Weiler, M., 2014. Karst water resources in a changing world: Review of hydrological modeling approaches. Rev. Geophys. 52, 218–242. https://doi.org/10.1002/2013RG000443.

Hauns, M., Jeannin, P.Y., Atteia, O., 2001. Dispersion, retardation and scale effect in tracer breakthrough curves in karst conduits. J. Hydrol. 241 (3–4), 177–193.

Jourde, H., Lafare, A., Mazzilli, N., et al., 2014. Flash flood mitigation as a positive consequence of anthropogenic forcing on the groundwater resource in a karst catchment. Environ. Earth. Sci. 71, 573–583. https://doi.org/10.1007/s12665-013-2678-3.

Käss, W., Tracing Technique in Geohydrology, A. A. Balkema, Brookfield, Vt., 1998.

Kaufmann, G., Romanov, D., Hiller, T., 2010. Modeling three-dimensional karst aquifer evolution using different matrix-flow contributions. J. Hydrol. 388 (3–4), 241–250.

Kincaid, T.R., Hazlett, T.J., Davies, G.J., 2005, Quantitative groundwater tracing and effective numerical modeling in karst—An example from the Woodville Karst Plain of North Florida. In: Beck, B.F., ed., Sinkholes and the engineering and environmental impacts of karst, Proceedings of the 10th Multidisciplinary Conference, San Antonio, Texas, September 24–28, 2005: Geological Institute of the American Society of Civil Engineers, Geotechnical Special Publication no. 144, p. 114–121.

Kiraly, L., 1998. Modelling karst aquifers by the combined discrete channel and continuum approach. Bull. D'hydrogéologie 16, 77–98.

Kordilla, J., Sauter, M., Reimann, T., Geyer, T., 2012. Simulation of saturated and unsaturated flow in karst systems at catchment scale using a double continuum approach. Hydrol. Earth Syst. Sci. 16 (10), 3909–3923.

Kumar, A., Dalal, D.C., 2014. Analytical solution and analysis for solute transport in streams with diffusive transfer in the hyporheic zone. J. Hydro Environ. Res. 8 (1), 62–73.

Léonardi, V., Jourde, H., Dausse, A., Dörfliger, N., Brunet, P., Maréchal, J.C., 2013. Apport de nouveaux traçages et forages à la connaissance hydrogéologique de l'aquifère karstique du Lez. Karstologia 62, 7–14.

Mazzilli, N. Sensitivity and uncertainty in karst hydrosystem modelling. Hydrology. Université Montpellier II - Sciences et Techniques du Languedoc, 2011. English. NNT: tel-00671069.

Morales, T., Uriarte, J.A., Olazar, M., Antigüedad, I., Angulo, B., 2010. Solute transport modelling in karst conduits with slow zones during different hydrologic conditions. J. Hydrol. 390 (3–4), 182–189.

Padin, A., 2016. Experimental and Theoretical Study of Water And Solute Transport Mechanisms in Organic-Rich Carbonate Mudrocks. Doctoral dissertation, PhD Thesis. Colorado School of Mines, Colorado, USA.

Roubinet, D., Dreuzy, J.R., Tartakovsky, D.M., 2012. Semi-analytical solutions for solute transport and exchange in fractured porous media. Water Resour. Res. 48 (1), 1–10.

Sharma, P.K., Joshi, N., Ojha, C.S.P., 2013. Stochastic numerical method for analysis of solute transport in fractured porous media. J. Hydro Environ. Res. 7 (1), 61–71.

Smart, C., 1988. Artificial tracer techniques for the determination of the structure of conduit aquifers. Ground Water 26 (4), 445–453.

Teutsch, G., Sauter, M., 1998. Distributed parameter modelling approaches in karst hydrological investigations. Bull. D'hydrogéologie 16, 99–109.

Weill, S., Mazzia, A., Putti, M., Paniconi, C., 2011. Coupling water flow and solute transport into a physically-based surface–subsurface hydrological model. Adv. Water Resour. 34 (1), 128–136.

White, W.B., 1999. Conceptual models for karstic aquifers. Karst Modeling 5, 11–16.

White, W. B. 1988. Geomorphology and hydrology of karst terrains.

Worthington, S.R., 2009. Diagnostic hydrogeologic characteristics of a karst aquifer (Kentucky, USA). Hydrogeol. J. 17 (7), 1665–1678.

Zhao, Z., Jing, L., Neretnieks, I., Moreno, L., 2011. Numerical modeling of stress effects on solute transport in fractured rocks. Comput. Geotech. 38 (2), 113–126.